

# Waveguide-integrated telecom-wavelength photodiode in deposited silicon

Kyle Preston,<sup>1,\*</sup> Yoon Ho Daniel Lee,<sup>1</sup> Mian Zhang,<sup>1</sup> and Michal Lipson<sup>1,2</sup>

<sup>1</sup>School of Electrical and Computer Engineering, Cornell University, Ithaca, New York 14853, USA

<sup>2</sup>Kavli Institute at Cornell for Nanoscale Science, Cornell University, Ithaca, New York 14853, USA

\*Corresponding author: [kjp32@cornell.edu](mailto:kjp32@cornell.edu)

Received August 24, 2010; revised November 16, 2010; accepted November 18, 2010;  
posted December 2, 2010 (Doc. ID 133850); published December 23, 2010

We demonstrate photodiodes in deposited polycrystalline silicon at 1550 nm wavelength with 0.15 A/W responsivity, 40 nA dark current, and gigahertz time response. Subband absorption is mediated by defects that are naturally present in the polycrystalline material structure. The material exhibits a moderate absorption coefficient of 6 dB/cm, which allows the same microring resonator device to act as both a demultiplexing filter and a photodetector. We discuss the use of deposited silicon-based complementary metal-oxide semiconductor materials for nanophotonic interconnects. © 2010 Optical Society of America

OCIS codes: 040.5160, 130.3130, 130.3120.

The crystalline silicon-on-insulator (SOI) platform enables modulation and low-loss waveguiding in the telecommunication wavelength bands centered at  $\lambda = 1.3 \mu\text{m}$  and  $1.55 \mu\text{m}$ . These functions can be implemented because of the 1.12 eV bandgap of bulk crystalline Si, which only produces significant linear absorption for  $\lambda < 1.1 \mu\text{m}$ . To add IR photodetection to silicon photonic circuits, germanium can be integrated as an absorbing material in complementary metal-oxide semiconductor (CMOS) processing environments, and several groups [1] have achieved very good photodetector characteristics with high responsivity  $\sim 1$  A/W, low dark current, and high speed  $\sim 40$  GHz. However, epitaxial growth of Ge-on-Si requires complex processing steps to manage the 4% lattice mismatch between the two crystals.

It is known that silicon can generate photocarriers via subband absorption of light with  $\lambda > 1.1 \mu\text{m}$  when defects are present that contribute energy states within the bandgap [2,3]. For integrated SOI devices, surface state absorption can produce a relatively low responsivity  $R = 0.036$  A/W in thin waveguides [4]. Bradley *et al.* and Logan *et al.* showed that the absorption can be further enhanced by distributing defects throughout the waveguide by ion implantation [5,6]. By engineering the defects and reducing the device size to a submicrometer cross-section, Geis *et al.* demonstrated photodetectors with  $R \gg 1$  A/W (with avalanche enhancement) and bandwidth  $> 30$  GHz in different device configurations [7]. Recently, the device size has been reduced by using a microring resonator for multiple round trips of light through the same implanted region [8,9], but all demonstrations to date have required single-crystalline SOI as a starting material.

Here we show photodiodes in polycrystalline silicon (polysilicon), a standard deposited material that can be integrated in the CMOS material stack. The use of deposited silicon-based materials can enable new flexibility in system architecture and chip fabrication [10]. We have previously used polysilicon to build integrated optical filters and electro-optic modulators [11] for monolithic integration of optical functionality onto a microelectronic chip. The results presented here demonstrate that at least 12% of the propagation loss in these submicrometer poly-

silicon waveguides is due to subband absorption that generates useful photocarriers. Polysilicon can therefore be used for both the modulator and photodetector at the start and end of an optical link on a CMOS chip.

We design photodetectors with an integrated p-i-n diode to sweep out generated carriers and a ring resonator geometry to reduce the footprint. The fabrication is similar to [11] with a summary as follows. We use  $3 \mu\text{m}$  oxide as a lower cladding, deposit 270 nm of high quality amorphous silicon by low-pressure chemical vapor deposition, and crystallize the material into polysilicon by a furnace anneal in  $\text{N}_2$  at  $1100^\circ\text{C}$  to maximize the grain size (see Fig. 3 in [12]). We perform moderate *n*-type phosphorus doping to an average concentration of  $2 \times 10^{17} \text{ cm}^{-3}$ . Many of the dopant ions and donor electrons are trapped at the material grain boundaries [13]. We pattern waveguides and resonators using *e*-beam lithography, etch the devices to leave a 40 nm slab for electrical access, and dope *p*+ and *n*+ contact regions. We clad the devices in silicon dioxide by plasma-enhanced chemical vapor deposition and make electrical contact with nickel silicide and aluminum. The device is shown in Fig. 1. The waveguide width is 550 nm, and the ring radius is  $50 \mu\text{m}$  to maximize the quality factor  $Q$  (minimize the bending and scattering loss) while maintaining a small footprint.

The optical loss through the sample and test setup must be carefully measured to determine accurate values

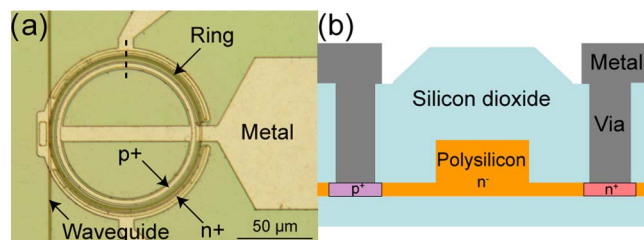


Fig. 1. (Color online) (a) Optical microscope image of  $50 \mu\text{m}$  radius polysilicon ring resonator with bus waveguide and metal contacts. (b) Cross-sectional schematic of the electro-optic device region (not to scale). Carriers are generated in the  $550 \text{ nm}$  wide waveguide region and extracted to the external circuit through the  $40 \text{ nm}$  slab.

of internal detector responsivity. Measurements are performed by coupling light into the waveguide using a tapered lensed fiber and collecting the waveguide output with an objective lens. A polarization controller is used before the chip to select the TM polarization, and a polarization filter is used after the chip. We calculate the waveguide propagation loss to be  $\alpha_{\text{wg}} = 34.6$  dB/cm by launching light onto the chip from either direction as follows. Launching from the first facet, we find the photocurrent on resonance to be  $I_1 = RP_{\text{in}1}C_{\text{in}}(\exp(-\alpha_{\text{wg}}L_1))(1 - T_{\text{min}})$ , and, launching from the other facet, we find  $I_2 = RP_{\text{in}2}C_{\text{in}}(\exp(-\alpha_{\text{wg}}L_2))(1 - T_{\text{min}})$ , where  $R$  is the internal responsivity,  $P_{\text{in}1}$  ( $P_{\text{in}2}$ ) is the power at the fiber tip for facet 1 (facet 2),  $C_{\text{in}}$  is the fiber-to-chip coupling efficiency,  $L_1$  ( $L_2$ ) is the propagation distance from facet 1 (facet 2) to the device,  $T_{\text{min}}$  is the on-resonance extinction ratio, and  $(1 - T_{\text{min}})$  is the fraction of power dropped into the ring. The equations reduce to  $I_1/I_2 = P_{\text{in}1}\exp(-\alpha_{\text{wg}}L_1)/P_{\text{in}2}\exp(-\alpha_{\text{wg}}L_2)$ , and we solve for  $\alpha_{\text{wg}} = 34.6$  dB/cm, which is primarily due to scattering but also includes useful absorption. Then, by measuring the total chip insertion loss and subtracting the propagation loss, we find the total chip coupling loss (input facet plus output facet) to be 12.9 dB. We conservatively assume half of this coupling loss to be at the input facet. Additionally, there is 1.8 dB propagation loss from facet 1 to the device, resulting in a total loss of 8.3 dB between the fiber tip and the device for the following measurements.

We determine the internal responsivity of the photodiode to be as high as 0.15 A/W. Figure 2(a) shows the transmission and measured current when we sweep the laser wavelength with a dc reverse bias on the device. When light is on resonance and trapped in the ring, it either scatters away or it is absorbed and generates photocurrent. Figure 2(b) shows the resonant photocurrent at  $-13$  V. The optical power in the bus waveguide at

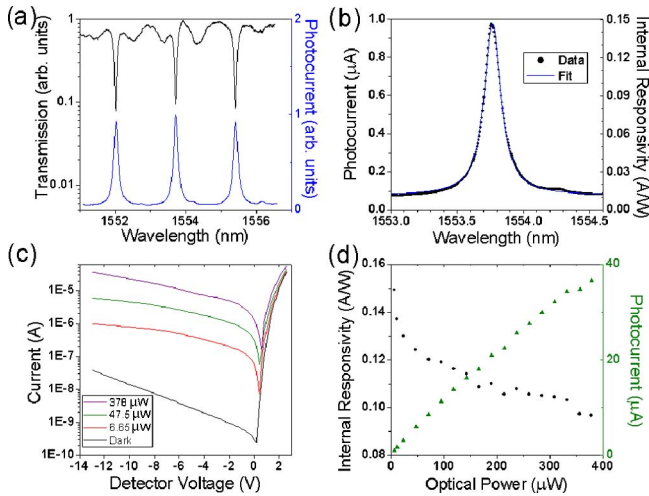


Fig. 2. (Color online) (a) Transmission and photocurrent spectra. (b) Close scan of resonance with  $6.7 \mu\text{W}$  optical power coupled into the device at  $-13$  V bias, demonstrating  $Q = 10,500$ . Solid curve is a Lorentzian fit. (c) Current-voltage characteristics under dark and light conditions, with wavelength set to resonance peak. Legend, optical power coupled into the device. (d) Responsivity (circles) and photocurrent (triangles) at  $-13$  V versus optical power coupled into the device, with wavelength set to resonance peak.

the device is  $P_{\text{wg}} = 7.35 \mu\text{W}$ , and the transmission extinction ratio is  $(1 - T_{\text{min}}) \times 100\% = 90.5\%$ , so  $P_{\text{det}} = (1 - T_{\text{min}}) \times P_{\text{wg}} = 6.65 \mu\text{W}$  is coupled into the resonator. We find a quality factor  $Q = 10,500$  and a maximum photocurrent  $I = 0.975 \mu\text{A}$  corresponding to internal responsivity  $R = 0.15$  A/W. The microring device acts as a wavelength-selective photodetector, which can both demultiplex and detect one wavelength of a WDM signal. This combined functionality is not possible in strongly absorbing materials where high loss would prevent the formation of a high- $Q$  resonance.

The responsivity of the photodiode is determined by the efficiency of both carrier generation (given by the ratio of absorption loss to total propagation loss in polysilicon) and carrier extraction. The absorption is due to dangling bonds, which produce a distribution of trap states slightly below the midbandgap energy [13,14], many of which are filled by donor electrons [6]. It is likely that, in this device, the photocarrier generation is primarily due to the phosphorus donor electrons being promoted from these trap states to the conduction band.

We measure a low dark current of 40 nA at an operating voltage of  $-13$  V. Figure 2(c) shows current-voltage curves with and without light coupled to the device with the wavelength on resonance. The photocurrent does not plateau but rather continues increasing with reverse bias voltage. This can likely be improved by placing contacts closer to where the carriers are generated or by tailoring the dopant concentration to ensure full depletion of the waveguide region. Note that we are not operating in an avalanche regime, which produces rapidly increasing dark current for  $V < -14$  V. Figure 2(d) shows responsivity as a function of the optical power coupled into the device at a bias voltage of  $-13$  V. We find that the internal responsivity decreases from 0.15 A/W to 0.10 A/W as the optical power is increased over nearly 2 orders of magnitude. This indicates that either the generation or extraction of carriers is suppressed at higher photocarrier densities in the device and that these effects are larger than any two-photon absorption effect, which would increase the responsivity.

We measure the transient response of the photodiode by modulating the cw laser with an external modulator. Figure 3(a) shows the direct output of the photodiode operating at a bit rate of 2.5 Gbps. To obtain an eye diagram, we amplify the photodiode output with a low-noise amplifier with 1 GHz bandwidth. An open eye diagram at

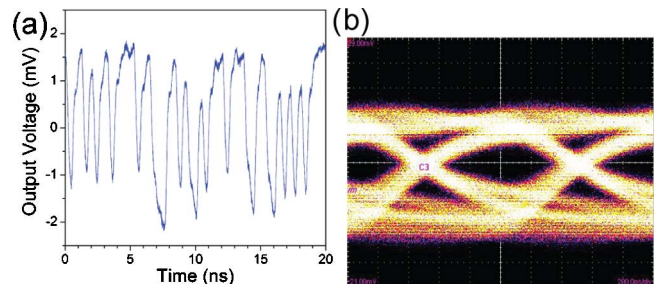


Fig. 3. (Color online) (a) Direct ac output of the photodetector on a sampling oscilloscope with a 2.5 Gbps  $2^7 - 1$  PRBS (pseudorandom bit sequence) input optical signal. (b) Amplified electrical output eye diagram at 1 Gbps. Scale: 200 ps/div, 5 mV/div.

1 Gbps is shown in Fig. 3(b). We measure the device  $S_{11}$  response using an HP8722ES vector network analyzer and find that the speed of the relatively large device is RC-limited. A circuit model and parameter fit is used to de-embed the parasitic contribution of contact pads, and we find the junction capacitance to be  $100 \text{ fF} \pm 7 \text{ fF}$  and series resistance to be  $524 \Omega \pm 25 \Omega$ . From these values, we determine the electrical bandwidth of the device and pads terminated into a  $50 \Omega$  load to be  $2.6 \pm 0.24 \text{ GHz}$ , which can be improved by engineering the device structure, reducing the size of the resonator, or integrating directly with a transimpedance amplifier.

We calculate the absorption coefficient  $\alpha_{\text{abs}} \geq 6 \text{ dB/cm}$  inside the device. The use of a near critically coupled resonator photodiode is equivalent to a long waveguide photodiode; photons in the cavity that do not scatter away must be absorbed. The measured quantum efficiency  $\text{QE} = 12\%$  (for  $R = 0.15 \text{ A/W}$  at  $\lambda = 1.55 \mu\text{m}$ ) is therefore a lower bound for  $\alpha_{\text{abs}}/\alpha_{\text{ring}}$ , the percent of propagation loss in the ring which is due to absorption. From the  $Q$  and extinction ratio, we calculate the total propagation loss in the ring (absorption and scattering) to be  $\alpha_{\text{ring}} = 51.7 \text{ dB/cm}$ , and the absorption coefficient is therefore  $\alpha_{\text{abs}} \geq 6.2 \text{ dB/cm}$ . We note that the actual absorption value is higher by the percentage of carriers that recombine before being extracted to the external circuit. Additionally, an identical photodiode integrated into a straight waveguide instead of a resonator could have a maximum  $\text{QE} = \alpha_{\text{abs}}/\alpha_{\text{wg}} = (6.2 \text{ dB/cm})/(34.6 \text{ dB/cm}) = 18\%$ , based on the measured straight waveguide loss. The responsivity can be enhanced by optimizing the background dopant type and concentration.

The polysilicon photodetector presented here can be integrated with CMOS SOI optical components for optical interconnect applications. However, these results also open the door to an integrated optical link which does not require any crystalline SOI material, as discussed in [15], but utilizes only silicon-based materials deposited in the CMOS stack. Both the modulator [11] and photodetector can be fabricated from the same polysilicon material. Absorption can be suppressed in the modulator regions by hydrogen passivation [10] and enhanced in the detector by optimizing the dopant type and concentration. Additionally, propagation loss in deposited silicon nitride has been demonstrated as low as  $0.1 \text{ dB/cm}$  [16], approximately 20 times better than losses in single-mode submicrometer crystalline SOI waveguides. Because of the ultralow optical loss, it may be possible to design optical links or networks whose system-level characteristics outperform the traditional SOI platform, even with some degradation in mod-

ulator and detector device performance as compared to SOI and crystalline Ge-on-Si.

In conclusion, we have demonstrated an integrated photodiode in polysilicon, a deposited CMOS material. The polysilicon exhibits  $6 \text{ dB/cm}$  absorption, which results in a responsivity of  $0.15 \text{ A/W}$ . We demonstrated  $2.5 \text{ Gbps}$  operation of the device and suggest several areas of research for achieving devices with even higher performance.

This work was supported in part by Intel Corporation (supervised by M. Reshotko) and the Cornell Center for Nanoscale Systems [supported by the National Science Foundation (NSF) and the New York State Office of Science, Technology and Academic Research] and was performed in part at the Cornell NanoScale Facility, a member of the National Nanotechnology Infrastructure Network, which is supported by the NSF.

## References

1. J. Michel, J. Liu, and L. C. Kimerling, *Nat. Photon.* **4**, 527 (2010).
2. H. Y. Fan and A. K. Ramdas, *J. Appl. Phys.* **30**, 1127 (1959).
3. M. Wolf, *Proc. IRE* **48**, 1246 (1960).
4. T. Baehr-Jones, M. Hochberg, and A. Scherer, *Opt. Express* **16**, 1659 (2008).
5. J. D. B. Bradley, P. E. Jessop, and A. P. Knights, *Appl. Phys. Lett.* **86**, 241103 (2005).
6. D. Logan, P. E. Jessop, and A. P. Knights, *J. Lightwave Technol.* **27**, 930 (2009).
7. M. W. Geis, S. J. Spector, M. E. Grein, J. U. Yoon, D. M. Lennon, and T. M. Lyszczarz, *Opt. Express* **17**, 5193 (2009).
8. J. K. Doyle, P. E. Jessop, and A. P. Knights, *Opt. Express* **18**, 14671 (2010).
9. S. Roshanak, Z. Dawei, L. Shirong, D. Po, L. Hong, F. Ning-Ning, B. J. Luff, F. Dazeng, L. Guoliang, C. John, R. Kannan, V. K. Ashok, and A. Mehdi, in *Optical Fiber Communication Conference*, OSA Technical Digest (CD) (Optical Society of America, 2010), paper OMI8.
10. L. Liao, D. R. Lim, A. M. Agarwal, X. Duan, K. K. Lee, and L. C. Kimerling, *J. Electron. Mater.* **29**, 1380 (2000).
11. K. Preston, S. Manipatruni, A. Gondarenko, C. B. Poitras, and M. Lipson, *Opt. Express* **17**, 5118 (2009).
12. K. Preston, P. Dong, B. Schmidt, and M. Lipson, *Appl. Phys. Lett.* **92**, 151104 (2008).
13. T. Kamins, *Polycrystalline Silicon for Integrated Circuits and Displays*, 2nd ed. (Kluwer, 1998).
14. W. B. Jackson, N. M. Johnson, and D. K. Biegelsen, *Appl. Phys. Lett.* **43**, 195 (1983).
15. I. A. Young, E. Mohammed, J. T. S. Liao, A. M. Kern, S. Palermo, B. A. Block, M. R. Reshotko, and P. L. D. Chang, *IEEE J. Solid-State Circuits* **45**, 235 (2010).
16. A. Gondarenko, J. S. Levy, and M. Lipson, *Opt. Express* **17**, 11366 (2009).